Planetary and Space Science 113-114 (2015) 193–204

Contents lists available at ScienceDirect

Planetary and Space Science

journal homepage: www.elsevier.com/locate/pss

Venus mesospheric sulfur dioxide measurement retrieved from SOIR on board Venus Express

A. Mahieux [a,b,*], A.C. Vandaele [a], S. Robert [a], V. Wilquet [a], R. Drummond [a], S. Chamberlain [a], D. Belyaev [c,d], J.L. Bertaux [e,f]

[a] Planetary Aeronomy, Belgian Institute for Space Aeronomy, 3 av. Circulaire, B-1180 Brussels, Belgium
[b] Fonds National de la Recherche Scientifique, rue d'Egmont 5, B-1000 Brussels, Belgium
[c] Space Research Institute (IKI), 84/32 Profsoyuznaya Street, 117997 Moscow, Russia
[d] Moscow Institute of Physics and Technology (MIPT), 9 Institutskiy per., Dolgoprudny, Moscow, 141700, Russia
[e] LATMOS, 11 Bd d'Alembert, 78280 Guyancourt, France
[f] Institut Pierre Simon Laplace, Université de Versailles-Saint-Quentin, 78280 Guyancourt, France

ARTICLE INFO

Article history:
Received 27 February 2014
Received in revised form
5 September 2014
Accepted 4 December 2014
Available online 17 December 2014

Keywords:
Planetary atmosphere
Venus
Composition
SO_2

ABSTRACT

SOIR on board Venus Express sounds the Venus upper atmosphere using the solar occultation technique. It detects the signature from many Venus atmosphere species, including those of SO_2 and CO_2. SO_2 has a weak absorption structure at 4 μm, from which number density profiles are regularly inferred. SO_2 volume mixing ratios (VMR) are calculated from the total number density that are also derived from the SOIR measurements. This work is an update of the previous work by Belyaev et al. (2012), considering the SO_2 profiles on a broader altitude range, from 65 to 85 km. Positive detection VMR profiles are presented. In 68% of the occultation spectral datasets, SO_2 is detected. The SO_2 VMR profiles show a large variability up to two orders of magnitude, on a short term time scales. We present mean VMR profiles for various bins of latitudes, and study the latitudinal variations; the mean latitude variations are much smaller than the short term temporal variations. A permanent minimum showing a weak latitudinal structure is observed. Long term temporal trends are also considered and discussed. The trend observed by Marcq et al. (2013) is not observed in this dataset. Our results are compared to literature data and generally show a good agreement.

1. Introduction

Sulfur dioxide was first detected in the Venusian upper atmosphere from Earth-based ultraviolet (UV) observations with a mixing ratio between 0.02 and 0.5 ppmv at the cloud top (Barker, 1979). Space-based identifications of SO_2 UV absorption followed soon from Pioneer Venus orbiter (PVO). These observations as well as those of Venera-15 showed a steady decline of the cloud top SO_2 content from 500 ppbv down to 20–50 ppbv about 2 years later (Esposito et al., 1997). The decline of the quantity of SO_2 was quite rapid over the first year, and much slower later on. This behavior was interpreted as a massive "injection" of SO_2 into the Venus middle atmosphere by a volcanic eruption (Esposito et al., 1997, 1988). Current observations performed by SPICAV-UV on board Venus Express (VEx) show that the high levels of SO_2 are again observed (Marcq et al., 2011, 2013).

Detailed thermochemical modeling indicates that (i) Volcanic outgassing is the most probable primary source of sulfur dioxide in Venus' lower atmosphere, even if no volcanic activity has been directly observed so far, and (ii) OCS and H_2S are likely formed via pyrrhotite oxidation (Fegley et al., 1997). The exchange of SO_2 from the lower to the upper atmosphere is not fully understood, but undoubtedly involves convective transport, presumably in conjunction with Hadley cell circulation. Photochemical oxidation efficiently removes SO_2 from Venus' upper atmosphere leading to the formation of the sulfuric acid droplets making up the clouds and haze enshrouding the planet, and as result the SO_2 abundance drops to ppbv levels; SO_2 located below the cloud layer is effectively sequestered from photochemical reactions.

The H_2SO_4 clouds, extending from ~48–70 km are formed via the sulfur-oxidation cycle, which begins with SO_2 photolysis producing SO, O, O_2 and S, followed by the oxidation of SO_2 by O forming SO_3. SO_3 then reacts with H_2O forming H_2SO_4. Additionally, the distribution and abundance of the sulfur-oxide species provides an indirect measure of the structure and the dynamics of Venus' atmosphere. The sulfur-oxidation cycle is therefore one of the most important chemical cycles of the Venus' atmosphere.

Analysis of HST/STIS observations obtained on 28/12/2010, 22/01/2011 and 27/01/2011 (Jessup et al., 2012) indicates that

* Corresponding author.
E-mail address: arnaud.mahieux@aeronomie.be (A. Mahieux).

http://dx.doi.org/10.1016/j.pss.2014.12.011
0032-0633/

the cloud top SO_2 density was highest in December 2010 and decreased by a factor of ~10 one month later, but stayed within a factor of 2 between the two January 2011 observations. The range of SO_2:CO_2 gas mixing ratio inferred from the HST data is ~ 10–350 ppbv, consistent with abundances obtained from previous SPICAV and SOIR studies (Belyaev et al., 2012; Marcq et al., 2013). The HST/STIS observations showed a general trend of the SO_2 gas density decreasing as the latitude increased, also observed by the SPICAV-UV instrument (Marcq et al., 2011; Marcq et al., 2013); this analysis also indicated that the SO_2 density decreased with local time from the morning terminator towards noon, as expected for a photo-chemically controlled species.

Ground-based submm spectroscopic observations (JCMT) provide simultaneous measurements of SO_2 and SO mixing ratios (Sandor et al., 2007, 2010), as well as upper limits for H_2SO_4 (Sandor et al., 2012) in the Venus mesosphere (70–100 km), with altitude resolution of 5–30 km, depending on signal strength and altitude. JCMT altitude sensitivity does not overlap with cloud top observations of HST (Jessup et al., 2012), IRTF/TEXES (Encrenaz et al., 2012), or SPICAV-UV (Marcq et al., 2011). JCMT data show that the SO/SO_2 ratio is different on the day vs. night sides, but cannot characterize the twilight atmosphere independently. Diurnal coverage of JCMT does not overlap with that of SOIR and SPICAV-UV data, from Belyaev et al. (2012). Measurements from JCMT submm spectra are thus unique in their altitude and local time sensitivity, providing knowledge of Venus SO_2 behavior that is not available from any other source. SO_2 has been mapped using the IRTF/TEXES high-resolution spectrometer (Encrenaz et al., 2012) showing strong variations (factors of 5–10) over the disk of Venus. The position of the SO_2 maximum was shown to vary strongly in time with maximum mixing ratio varying between 75 ± 25 ppbv and 125 ± 50 ppbv on the scale of a day for 60–80 km altitudes. SO_2 measurements in the submm obtained with ALMA sees an increase of the SO_2 VMR above 80 km (Moullet et al., 2013), and suggests the presence of local sulfur-bearing aerosols sources at higher altitude.

SO_2 has been observed by VIRTIS (Marcq et al., 2008) and SPICAV-UV (Marcq et al., 2011) instruments on board VEx and also by SOIR (Belyaev et al., 2008, 2012), to which this paper is an update. SPICAV-UV is able to detect SO_2 either in nadir mode (Marcq et al., 2011, 2013) or in solar occultation (Belyaev et al., 2012). Cross-sections in the UV are much bigger than in the infrared (IR). SPICAV-UV occultations indicate the presence of an enhanced layer of SO_2 at 85–100 km altitude. Latitudinal dependence and temporal variability (from day to several years) was observed, hinting at long-term temporal changes in the Venus atmosphere. VIRTIS/VEx is able to measure SO_2 on the night side, but the relative accuracy is quite poor due to the narrow spectral signature of SO_2. As a consequence, VIRTIS is only able to confirm the average value for SO_2 mixing ratio near 30 km: 150 ppmv reported by Marcq et al. (2008). For SOIR, SO_2 absorption is weak in the IR and, in some cases this would result in the determination of detection limits rather than positive abundance measurements. To overcome this issue, a critical analysis and definition of objective criteria for positive detection is described in this work. SOIR is also sensitive to CO_2 and to temperature (Mahieux et al., 2015a,b).

The new analysis of measurements obtained with SOIR will help to improve the understanding of such processes, since it provides SO_2 number density and volume mixing ratio (VMR) vertical profiles in the 65–100 km region at the Venus terminator, covering all latitudes, in the period May 2006–February 2013.

In the following, the instrument and measurement technique are shortly described. The inversion procedure is explained and a sensitivity study is presented and discussed. Then, the dataset is presented, and the latitude and long term variations are studied.

2. Instrument and measurement description

The SOIR instrument has been extensively described in previous publications, see Nevejans et al. (2006), Bertaux et al. (2007), Mahieux et al. (2008, 2009, 2010) and Vandaele et al. (2013). Only a short summary will be given here. The instrument is an IR spectrometer, sensitive in the 2.29–4.43 μm region (2257–4430 cm^{-1}). The light diffraction is obtained using an echelle grating, splitting the light in 94 diffraction orders, ranging from 101 to 194. A TeO_2 Acousto-Optic Tunable Filter (AOTF) placed before the instrument entrance slit is used to select one of the diffraction orders. Its transfer function has a sinc-square shape. Initially, the AOTF width was designed to be equal to the echelle free spectral range (FSR, 21 cm^{-1}). But misalignment of the AOTF or cracks in the crystal, seem to have occurred during the launch of the spacecraft resulting in a full width at mid height of the filter larger than the FSR (24 cm^{-1}). Consequently, overlap of the orders adjacent to the targeted order is observed on the SOIR detector, modulated by the AOTF transfer function. Usually, three orders either side of the selected order need to be considered to correctly interpret a spectrum. The instrument resolution varies from 0.11 to 0.21 cm^{-1}, the spectral sampling from 0.061 to 0.117 cm^{-1} and the spectral interval on the detector from 19.4 to 37.2 cm^{-1}, with increasing order. The measurements have a high signal to noise ratio (SNR), varying from 500 to more than 3000, depending on the order scanned and on the latitude of the measurement (SNR decreases while going from the North Pole towards the South, because the distance between the planet and VEx increases).

SOIR sounds the Venus atmosphere using the solar occultation technique, looking at the Sun while the line of sight of the instrument crosses the Venus atmosphere as the VEx spacecraft moves along its orbit. As a consequence, SOIR measurements always occur at the terminator, on the morning side (6.00 AM) or evening side (6.00 PM). The vertical sampling and vertical resolution of the measurements are latitude dependent, where the vertical sampling is the vertical distance between the mean altitude of two successive soundings and the vertical resolution is the vertical altitude range sounded by the projected slit at the limb on the atmosphere at the time of a measurement. The vertical sampling is best at 45° North (200 m), which degrades to 2 km at the North Pole, and up to 5 km at the South Pole. The vertical resolution is best at the North Pole (200 m), and increases up to 5 km at the South Pole.

SOIR can measure up to four different diffraction orders during an occultation, allowing us to target different species quasi-simultaneously. The main Venus atmospheric gases have ro-vibrational signatures in the SOIR wavelength range, including CO_2 (Bougher et al., 2015; Mahieux et al., 2010, 2012, 2015a), CO (Vandaele et al., 2015), H_2O (Fedorova et al., 2008), HCl and HF (Mahieux et al., 2015b) and SO_2, topic of this work.

The altitude range probed extends from 65 km up 170 km for CO_2 and from 65 to 100 km for SO_2. VEx has an orbital period of 24 h, with its perigee occurring around midnight UTC-time. Orbit number 1 corresponds to the 22nd of April, 2006. Occultation seasons (OS) occur for a one to two month period every three to four months. The 25 first OS are considered in this work, from 27/05/2006 to 23/02/2013.

3. Sulfur dioxide spectroscopy and retrieval procedure

The sulfur dioxide signature is observed in the 2458–2525 cm^{-1} wavenumber region, which corresponds to three SOIR diffraction orders, 110, 111 and 112. Fig. 1 shows the SO_2 line intensities of the main isotopologue ($^{32}S^{16}O_2$) in this spectral region, together with four isotopologues of CO_2 ($^{12}C^{16}O_2$,

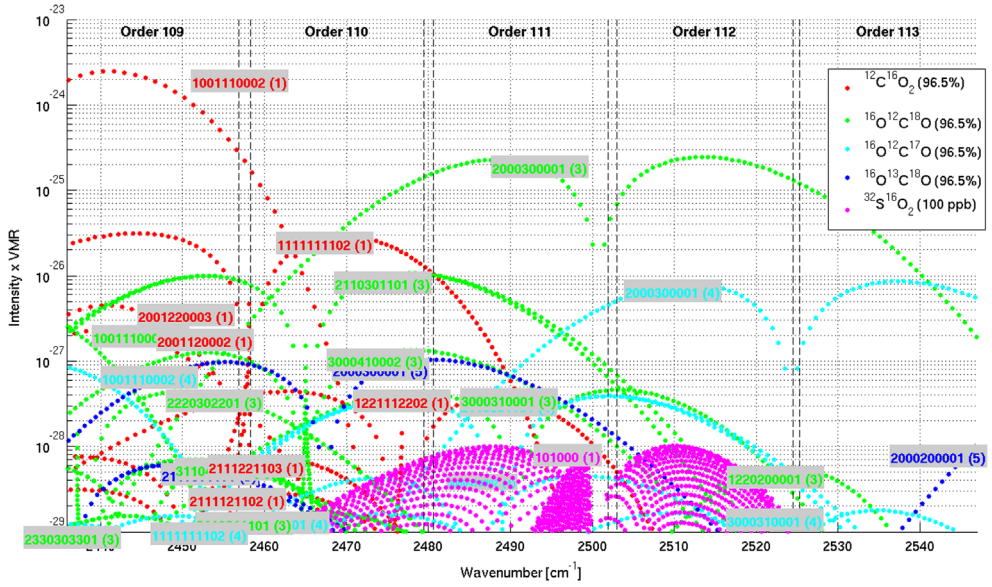

Fig. 1. Line parameters for SO_2 and CO_2 in the 2458–2525 cm^{-1} region obtained from HITRAN (Rothman et al., 2013). Four CO_2 isotopologues and the main isotopologue of SO_2 are presented. The intensities are multiplied by typical VMR for both species. The ro-vibrational transitions of the bands are also displayed, adopting the HITRAN notation. The lines intensities are already corrected for the Earth isotopic ratios in the HITRAN database; the Venus ratios are assumed to be the same (Bézard et al., 1987; Clancy and Muhleman, 1991; Rothman et al., 2013).

Table 1
List of the CO_2 and SO_2 bands absorbing in the 2458–2525 cm^{-1} wavenumber region, and that are above the noise level of the SOIR spectra. The first column gives the related species, the second column the absorbing band and the third column the diffraction orders in which they absorb.

Species	Band	Orders
$^{16}O^{12}C^{16}O$	$10^01(1)$-$10^00(2)$	110*, 111
	$11^11(1)$-$11^10(2)$	110–112
	$12^21(1)$-$12^20(2)$	110–112
	$20^01(2)$-$20^00(3)$	110
$^{16}O^{12}C^{18}O$	$20^00(3)$–$00^00(1)$	110*, 111*, 112*
	$21^10(3)$-$01^10(1)$	110*, 111*, 112
	$30^00(4)$-$10^00(2)$	110–112
	$30^00(3)$-$10^00(1)$	110–112
	$22^20(3)$-$02^20(1)$	110
$^{16}O^{12}C^{17}O$	$20^00(3)$-$00^00(1)$	110, 111*, 112*
	$21^10(3)$-$01^10(1)$	110–112
$^{16}O^{13}C^{18}O$	$20^00(3)$-$00^00(1)$	110–112
$^{32}S^{16}O_2$	101-001	110–112

$^{16}O^{12}C^{18}O$, $^{16}O^{12}C^{17}O$ and $^{16}O^{13}C^{18}O$), multiplied by typical VMRs of both species (100 ppbv and 96.5% respectively). The lines intensities are already corrected for the Earth isotopic ratios in the HITRAN database; the Venus ratios are assumed to be the same (Bézard et al., 1987; Clancy and Muhleman, 1991). The spectroscopic parameters and notation are from HITRAN (Rothman et al., 2013). The ro-vibrational notation is $v_1v_2^{l_2}v_3(r)$ for CO_2 and $v_1v_2v_3$ for SO_2 (Rothman, 1981; Rothman et al., 2005). The two first columns of Table 1 give the list of the isotopologues and the bands used in this work to simulate the SOIR spectra.

In this wavenumber region, from the HITRAN database, only SO_2 and CO_2 are above the SOIR detection limit: water has absorption lines from a weak band (max. intensity $\sim 10^{-25}$ $cm^{-1}/(molecule \times cm^{-2})$). N_2O (max. intensity $\sim 5 \times 10^{-21}$ $cm^{-1}/(molecule \times cm^{-2})$), HBr (max. intensity $\sim 2 \times 10^{-20}$ $cm^{-1}/(molecule \times cm^{-2})$) and C_2H_2 (max. intensity $\sim 7 \times 10^{-23}$ $cm^{-1}/(molecule \times cm^{-2})$) also have weak absorption bands, but were never observed in the Venus mesosphere or reported in Venus atmosphere chemistry models. All these species have or would have concentrations too low to be detectable in the SOIR spectra for the wavenumber region considered in this work.

4. Retrieval procedure

4.1. Method

The general method to obtain number density and temperature profiles has been presented in Mahieux et al. (2010), (2012), (2015a) and Vandaele et al. (2015); a summary is given here. The ASIMAT algorithm is an iterative program consisting of two main steps. In the first step, the Rodgers Bayesian method (Rodgers, 2000) is implemented in an onion peeling frame, considering spectra which show atmospheric non-saturated spectral structures only, and calculating independent number density profiles of the species that absorb in each of the orders measured during the occultation. A discretization of the slit projection in the atmosphere is implemented to correct for the vertical resolution variation with latitude (Mahieux et al., 2015a). In a second step, the independent number density profiles from the different orders are combined using a weighted linear moving average procedure (Mahieux et al., 2012; Vandaele et al., 2015). From the CO_2 number density profiles, we derive the temperature profiles using the hydrostatic law. The inversion is considered to have converged when both number density and temperature profiles are within the uncertainty of the previous step.

In the above procedure, the a-priori SO_2 VMR is set to 70 ppbv, constant with altitude, and the CO_2 VMR equal to the one from VIRA (Venus International Reference Atmosphere, from Hedin et al. (1983) and Zasova et al. (2006)).

To limit the dependence of the retrieved species density to the a-priori density profiles used in the Bayesian algorithm, only the number density values that were actually fitted for each profile are taken into account. This number is given by the degrees of freedom (DOF) of the retrieval extracted from the Rodgers averaging kernel matrix. It is equal to the trace of the averaging kernel matrix. DOF indicates the total number of independent variables that can be derived from the set of spectra. We only consider the layers corresponding to the DOF largest eigenvalues of the

averaging kernel matrix. In case of no SO_2 detection over the whole profile, its corresponding DOF is close to zero.

4.2. Specific procedure to derive SO_2 VMR profiles

We developed a specific procedure to derive SO_2, whose abundance is close to the detection limit:

(1) The CO_2 number density and the temperature profiles are obtained considering only the strongest CO_2 bands absorbing in the order. These are always observed above the noise level of the spectra. The orders in which these CO_2 bands occur are marked with a star in Table 1. The temperature profile is calculated on the CO_2 number density profile resulting from this fit using the ASIMAT algorithm.
(2) In a second step, SO_2 and CO_2 are fitted simultaneously with the ASIMAT algorithm considering all the CO_2 bands and the SO_2 band listed in Table 1. A set of independent SO_2 number density profiles are obtained, together with their uncertainties. The DOF criterion defined above is used to choose the points that are reliable measurements in each independent profile. Then, these resulting profiles are combined using the same procedure as in the ASIMAT algorithm (Mahieux et al., 2012), using a weighted linear moving average procedure across two scale heights. The resulting profile only contains positive detections.
(3) From these same independent SO_2 number density profiles, a SO_2 upper-limit profile is built. We consider all the points from each independent SO_2 number density profile derived from each order and each bin. The DOF criterion defined above is not used, and the profiles are combined using a weighted linear moving average procedure across two scale heights. These profiles are very dependent on the a-priori VMR profile used in the Bayesian retrieval algorithm. For this reason, they will not be discussed in the following.

4.3. Retrieval example

The procedure is illustrated in the following example, for occultation 235.1, during which orders 110, 111 and 112 were measured on 12/12/2006 at a latitude of 88 °N and local solar time of 6.00 PM.

First, the CO_2 number density profile is derived from the three measured orders, only considering the strong bands in the orders, listed with a star in Table 1, and taking atmospheric saturation into account. After convergence of the algorithm, the temperature profile is calculated using the hydrostatic law (Mahieux et al., 2012, 2015a). Both profiles are presented in the upper panels of Fig. 2 (A and B); panels C–J of the same figure show the quality of typical spectral fits – the middle panels (C–F) are observed and fitted spectra, lower panels (G–J) are spectral residuals. The second step is to fit the spectra considering all the CO_2 bands listed in Table 1 and SO_2 simultaneously. The regions where the independent SO_2 number density profiles from each order and each bin that satisfy the DOF criterion defined above are the solid tick colored profiles in Panel A. The errors on each independent profile range between 50 and 600%. The dashed profiles in the same panel are the whole profiles, showing the regions that do not satisfy the DOF criterion. The mean SO_2 number density profile is obtained from all the single measurements that satisfy the above mentioned DOF criterion, using the weighted linear moving average procedure across two scale heights (the bold solid black profile in Panel B of Fig. 3) that was calculated from the SO_2 number densities, presented as crosses in the plot. The horizontal bars are the final uncertainties, calculated as the weighted standard deviations from

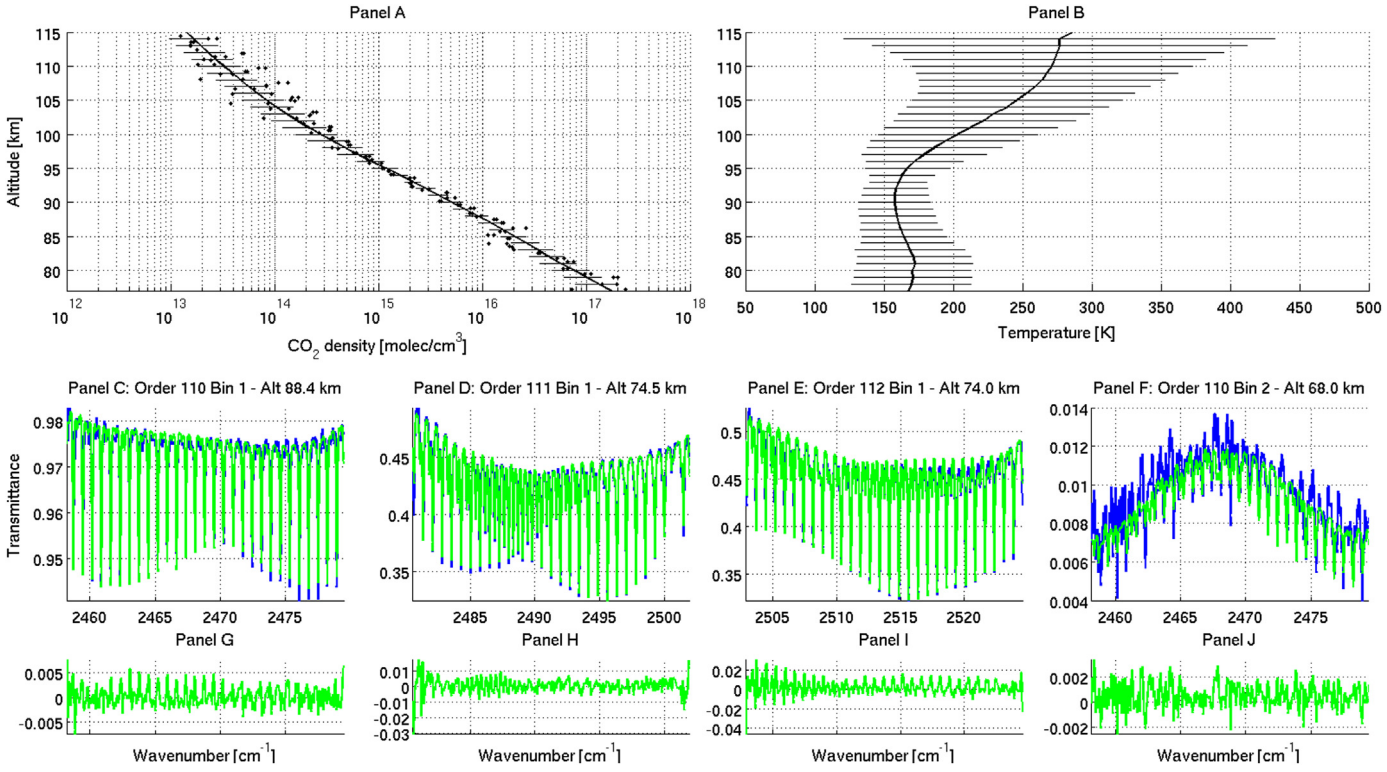

Fig. 2. Top panels: CO_2 number density (A) and temperature (B) profiles derived from orders 110–112 measured during orbit 235.1. In both panels, the horizontal lines are the uncertainties. In panel A, the dots are single measurements from the individual profiles used to build the mean density profile. Bottom panels: examples of spectral fits for different orders and bins, the altitude is given as an indication; in the upper insets (panels C–F), the blue spectra are the measured spectra, the green spectra are the fitted spectra; in the lower inset (panels G–J), the residuals of the fits are presented. (For interpretation of the references to color in this figure legend, the reader is referred to the web version of this article.)

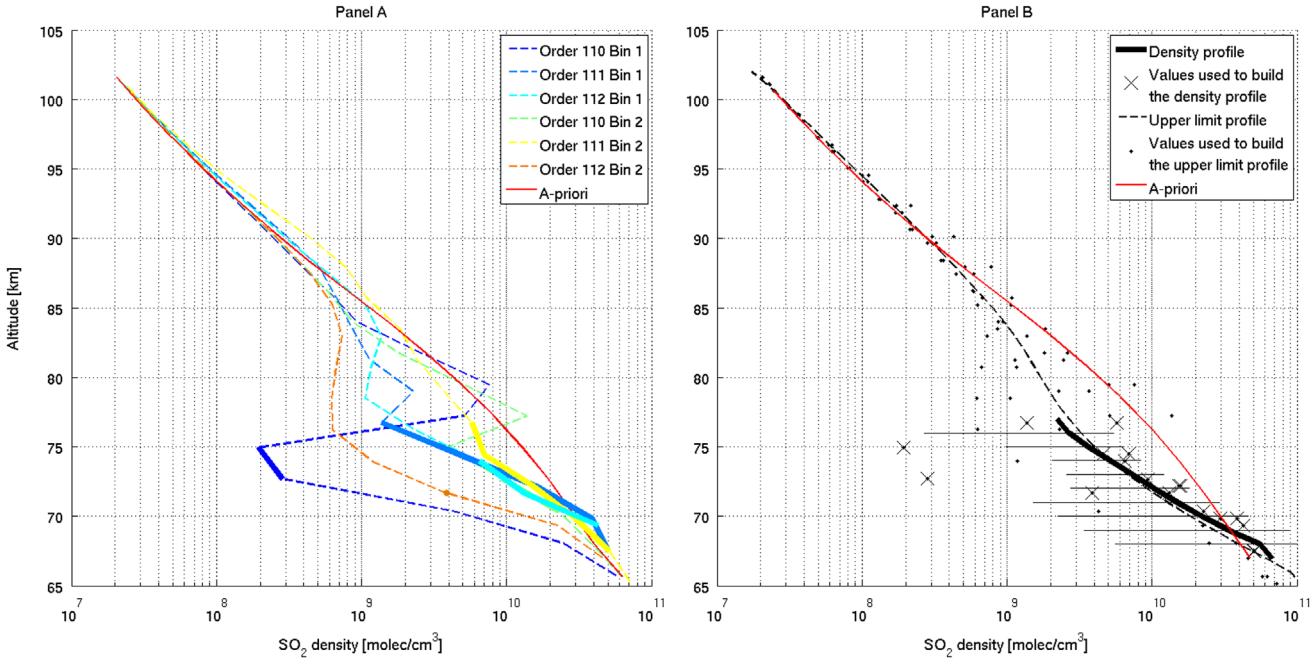

Fig. 3. Left panel (A): SO_2 upper limit profiles (dashed) and number density profiles (solid) from the 3×2 spectral sets measured during orbit 235.1 as a function of altitude. The a-priori profile is given as the red profile. Right panel (B): mean SO_2 number density profiles (black solid curve) calculated from the single measurements (crosses) that satisfy the DOF criterion defined elsewhere in this work. The horizontal lines are the uncertainties, calculated as the weighted standard deviations from single independent profiles from Panel A. The dashed profile is the mean SO_2 upper limit profile, calculated from all the SO_2 single measurements (dots). The a-priori profile is the red curve. (For interpretation of the references to color in this figure legend, the reader is referred to the web version of this article.)

single independent profiles. The uncertainty ranges between 24 and 96%; it is reduced from the individual profiles error by the weighted linear moving average procedure. The upper-limit profile is the dashed profile, calculated from all the SO_2 values, presented as dots in the plot.

The SO_2 VMR is also calculated by dividing the SO_2 number density profile by the total number density profile, which was in turn obtained from the CO_2 number density profiles calculated simultaneously by the ASIMAT algorithm (Mahieux et al., 2012, 2015a).

4.4. Sensitivity to the SNR discussion

To investigate the sensitivity of the retrieval to the SO_2 abundance, typical synthetic transmittance spectra have been calculated at an altitude of 75 km, for typical total and CO_2 number densities, and considering different SO_2 VMRs: 1 ppbv, 10 ppbv, 100 ppbv, 1 ppmv and 10 ppmv. Different SNR values on the spectra were also assumed: 100, 500, 1000, 2000 and 5000, which correspond to the typical range of values seen in the observed spectra. These simulated spectra are presented in Fig. 4, for the geometry and temperature and total density conditions of orbit 341 (28/03/2007, 82 °N, 6.00 PM). In Panel A, synthetic transmittance spectra $\tau_{CO_2+SO_2}$ (colored spectra) are calculated considering a CO_2 VMR of 96.5% and the different SO_2 VMRs, with noise added corresponding to the typical SNR values given above. They are compared to a CO_2 only synthetic transmittance spectrum τ_{CO_2} given in black. The differences between the synthetic $\tau_{CO_2+SO_2}$ spectra and the τ_{CO_2} spectrum are presented in Panel B. The equivalent noise level is shown as the horizontal dashed lines. It can be clearly seen that the SO_2 detection for low VMR values is highly dependent on the SNR value. Pure SO_2 spectra are presented in Panel C of the same figure. In Panel B, the spectral features are observed above the smallest noise for SO_2 VMRs as low as 10 ppbv. It should be noted that the spectral features are not from the SO_2 spectral signature only, since the subtraction of the CO_2 spectrum from the CO_2+SO_2 spectrum is not equal to a pure SO_2 spectrum τ_{SO_2}: $\tau_{CO_2+SO_2} - \tau_{CO_2} \neq \tau_{SO_2}$. This is due to the fact that non-linearity is introduced in the spectrum during the convolution of the spectra by the instrumental function and by the order addition (Mahieux et al., 2010).

The dependence of the SO_2 detection limit to the SNR value is addressed in the following. Synthetic spectra have been built for different SO_2 VMRs and typical CO_2. A CO_2 only spectrum is subtracted from these SO_2+CO_2 spectra. The resulting transmittance difference is transformed into an equivalent SNR. This operation is performed on spectra calculated at different altitude levels. The results are presented in Fig. 5 for order 112. The vertical axis is set as the total pressure, in order not to consider the large atmosphere variations that are observed at the terminator, that can reach up to two orders of magnitude for a given altitude level, see Mahieux et al. (2015a). The approximate altitude is given on the right hand side of the graph. SO_2 equivalent SNR are plotted for the different SO_2 VMRs in function of pressure (altitude). Such a plot can help us to discriminate between a positive detection (SO_2 abundance well above the detection level) and a non-detection. Let us consider, for example, the SNR value of 500, represented as one of the black thick lines: SO_2 can be observed down to a VMR of 3 ppbv at a pressure of 20 mbar (~71 km), down to 100 ppbv at a pressure of 0.25 mbar (~93 km) and 1 ppmv at a pressure of 0.02 mbar (~101 km). Such maps have been built for orders 110 and 111 too. The SO_2 VMR derived in the SOIR spectra presented in the following sections are in agreement with this SNR dependence.

4.5. Sensitivity to the a-priori discussion

In the Rodgers Bayesian formalism, the algorithm fits the logarithm of the species densities, i.e. $\log(VMR_{species} \times \rho_{tot})$, where ρ_{tot} is the total density profile. It uses as a-priori profiles the logarithm of number density of each species. The square root of the covariance matrix diagonal elements, which represent the amplitude of the variations allowed around the a-priori, are taken

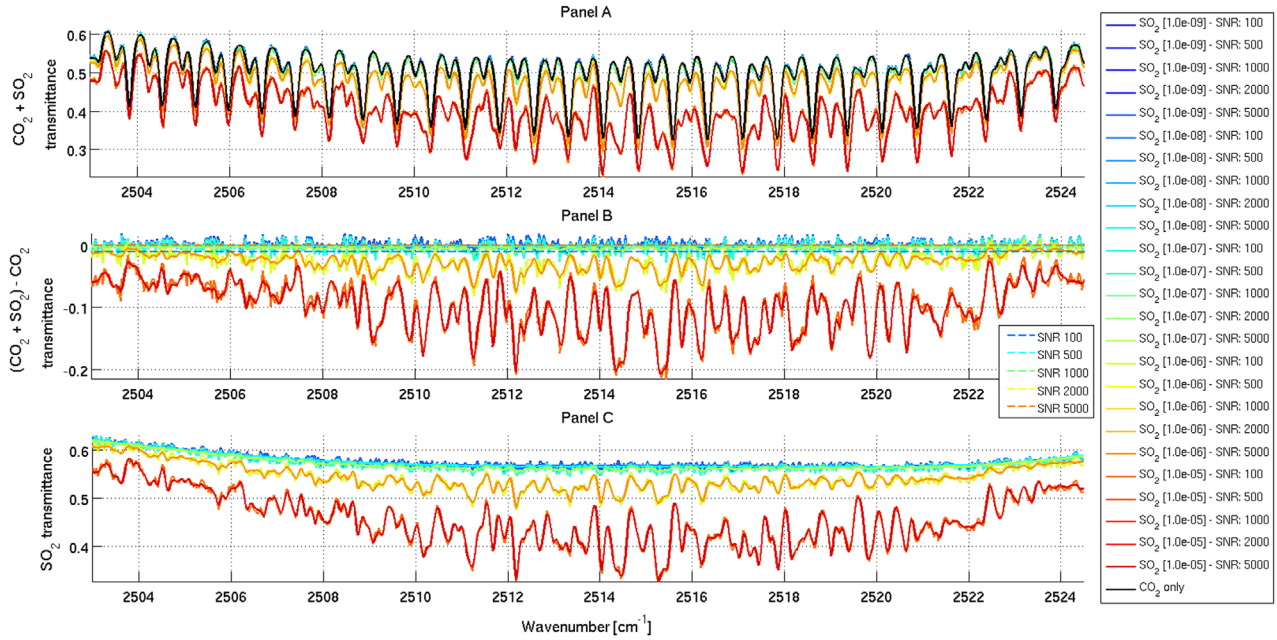

Fig. 4. SO_2 spectral signature in the SOIR spectra, example of order 112. Panel A: synthetic transmittances calculated at an altitude of 75 km for the atmospheric conditions derived during orbit 341.1. The CO_2 VMR is equal to 96.5% and the SO_2 VMRs are equal to 1 ppbv, 10 ppbv, 100 ppbv, 1 ppmv and 10 ppmv. White noise is added to the spectra, corresponding to SNR of 100, 500, 1000, 2000 and 5000. The colored spectra are for the different combinations of SO_2 VMRs and SNRs, the black spectra is for CO_2 only, with no SO_2. Panel B: synthetic spectra difference between the CO_2 and SO_2 spectra and the CO_2 only spectrum. The horizontal dashed color lines are the equivalent different SNR values. The color code is the same as in Panel A. Panel C: synthetic spectra calculated without CO_2, considering SO_2 only, for the different VMRs.

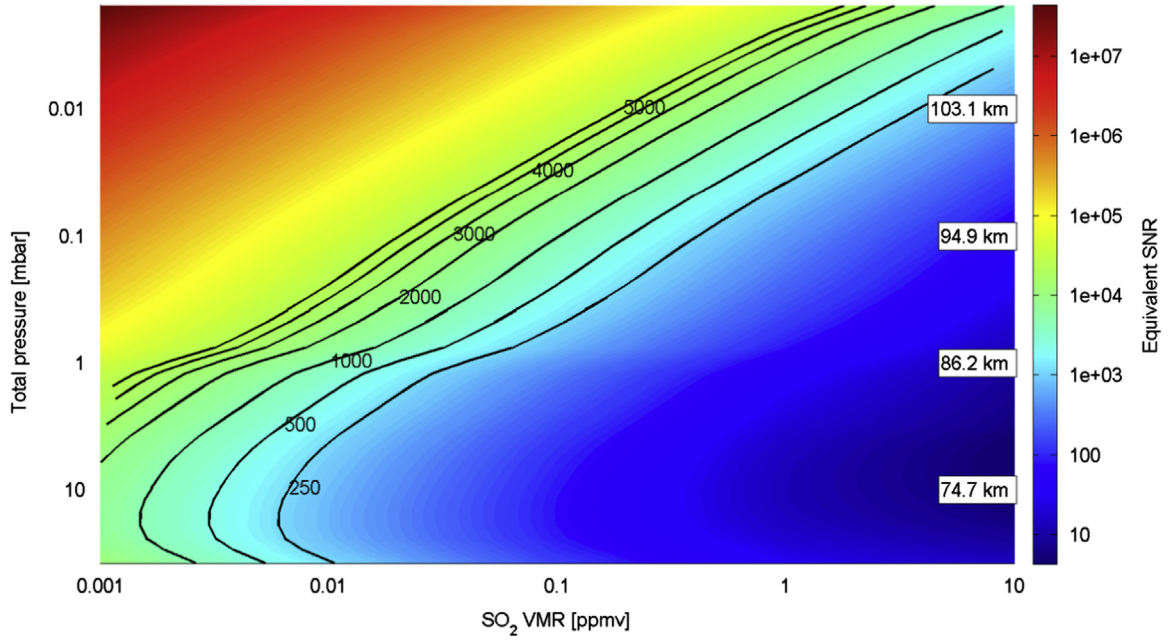

Fig. 5. Equivalent SNR for various SO_2 VMRS, varying from 1 ppbv to 10 ppmv, given as a function of the total pressure, the altitude is given on the right hand side as an indication. The equivalent SNR is calculated by converting the lines intensities of SO_2 present in the spectra into a noise level. Constant SNR curves are shown in black.

as 25% of the a-priori profile. This means that a valid solution is found only if the a-priori is close enough to it. In the following, the discussion will be held on VMR profiles, even if the fitted variable is the logarithm of the SO_2 number density profile.

To study the sensitivity to the a-priori SO_2 profiles, three cases are considered here, with different VMR constant profiles: 7 ppbv, 70 ppbv and 700 ppbv. The 70 ppbv is the standard case used in this work. These a-priori profiles have been used to fit SO_2 from the measurements of orbit 235.1 (same as in the example above), during which orders 110, 111 and 112 were recorded.

For the 7 ppbv a-priori profile, no detections are obtained: the fitted profile remains on the a-priori profile (not shown in Fig. 6). The variations allowed around the logarithm of the SO_2 a-priori number density profile are too small to encompass the "true solution".

Results are presented in Fig. 6 for the 70 ppbv and 700 ppbv a-priori VMRs. In the left panels of the figure, the independent number density profiles are shown as solid curves for the values satisfying the DOF criterion and dashed curves when considering all individual dots without the DOF criterion. The vertical

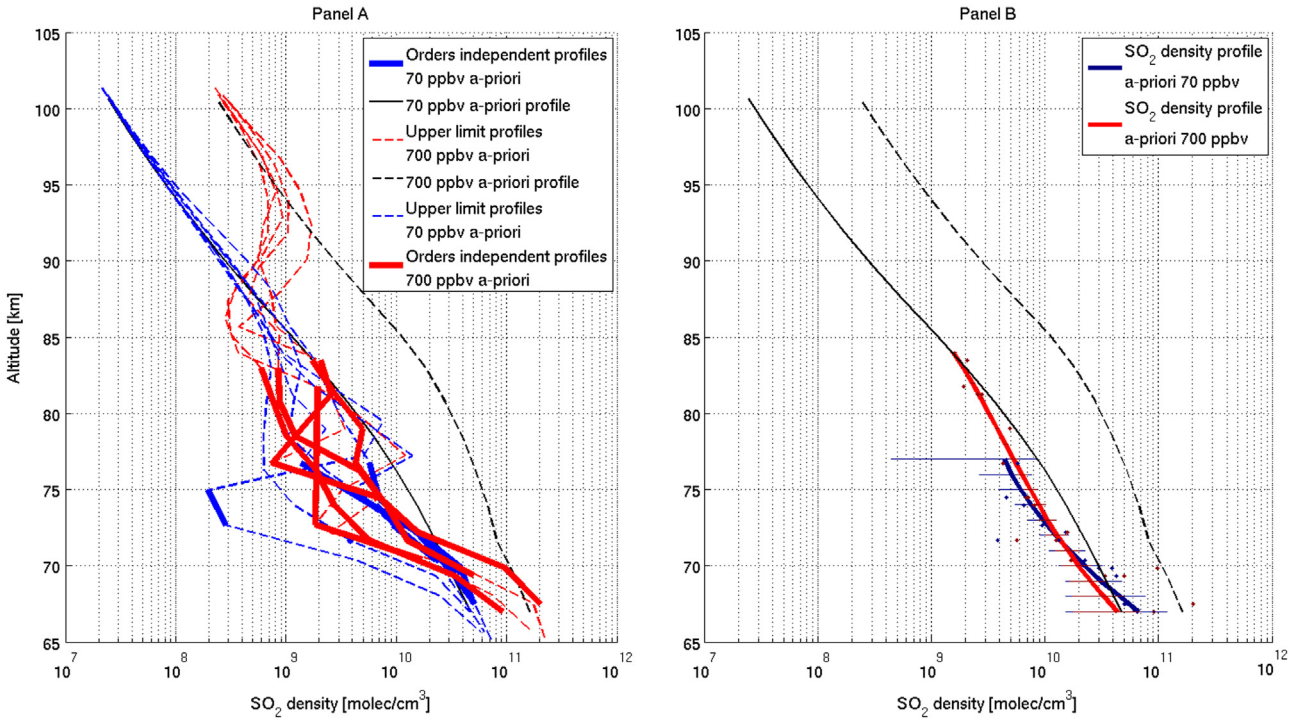

Fig. 6. Study of the sensitivity test towards the SO_2 a-priori VMR: two cases of constant VMR profiles are presented, 70 ppbv (blue) and 700 ppbv (red). Panel A: independent density profiles for the two cases. The solid thick profiles are the fitted profiles, i.e. the regions of the profiles that satisfy the DOF criterion; the dashed profiles are the remaining profiles, or upper-limit profiles; black lines are the SO_2 VMR a-priori profiles; solid line for 70 ppbv, dashed line for 700 ppbv. Panel B: mean profiles built from the independent data points of each case. (For interpretation of the references to color in this figure legend, the reader is referred to the web version of this article.)

extension of the region where the DOF criterion is satisfied is dependent on the a-priori; however the bulk of the positive detection, in this case 68–75 km, remains the same. The mean profiles are presented in panel B. They are both in agreement within their standard deviations.

We conclude that there is a weak dependence to the a-priori profile. However, as explained in the Rodgers method, the a-priori should be the 'best knowledge' of the solution and therefore should be realistically chosen.

5. Results and discussion

5.1. Dataset description

We applied the procedure described above on the SOIR database, which counts 137 solar occultations potentially containing a SO_2 signature. All the measurements were taken between 27/05/2006 and 23/02/2013 – corresponding to orbits 36.1 and 2500.1, and covering all latitudes from Pole to Pole. The measurements are always taken at 6.00 AM or 6.00 PM – both sides of the terminator. The 30 °N – 60 °N is poorly covered due to the geometry of the spacecraft orbit. Fig. 7 is a map of the measurement as a function of latitude and orbit number. In this figure, circles denote morning side measurements and triangles the evening ones. The color code is the absolute latitude: blue for the equatorial region, red at the Poles. The filled markers indicate that SO_2 has been detected during the occultation, while the unfilled ones represent a non-detection. 93 positive detections out of 137 are recorded, which represents 68% of the occultations.

The non-detections of SO_2 are mostly localized at latitudes lower than 60 °N. The SNR in the spectra of the measurements at these latitudes is larger than the SNR for measurements between the North Pole and 60 °N: this is because the distance to the planet is much larger, which induces a much coarser vertical sampling. 83% of the negative detections are found at latitudes lower than 60 °N. For this reason, it is hard to discuss the negative detections as a function of their latitude, time and terminator side. In the following, we only focus on the positive detection profiles.

Table 2 summarizes the number of measurements in the different latitude bins considered in this work, assuming latitudinal symmetry with respect to the Equator and a LST symmetry between dusk and dawn. The latitude regions, that will be used for binning the measurements, are chosen such that there is sufficient positive detections in each bin, to ensure statistic validity.

The individual SO_2 number density profiles are presented in panel A of Fig. 8. The vertical axis is the total pressure, to remove the global atmosphere variations with altitude; the approximate altitude is given on the right side of the plot. The points are SO_2 measurements that are obtained at a single altitude. The color code is the absolute latitude, and is the same as in Fig. 7. The error bars, not plotted for clarity, range between 40 and 200%, with a mean value of 81%. The SO_2 scale height varies between 2 km and 4.5 km. A large variability is observed at all altitude levels, with a geometric standard deviation factor (the standard deviation of an exponential variable) varying between 1.65 and 2.1 above 70 km and up to 3.4 at lower altitude.

The CO_2 profiles derived simultaneously are used to calculate the SO_2 VMR. The CO_2 variability in the Venus mesosphere at the terminator is large. It is extensively studied as a function of altitude, latitude and time in the companion paper (Mahieux et al., 2015a). The CO_2 profiles used in the present work have a geometric standard deviation equal to 2, and the temperature profiles have an arithmetic standard deviation of 31 K. The average uncertainty on the CO_2 density profiles varies between 4% and 20%; the largest uncertainties are found at the lowest altitude levels.

The individual SO_2 VMR profiles are presented in panel B of Fig. 8, calculated from the total density derived from the SOIR CO_2 profiles, and given as a function of the total pressure. Error bars are

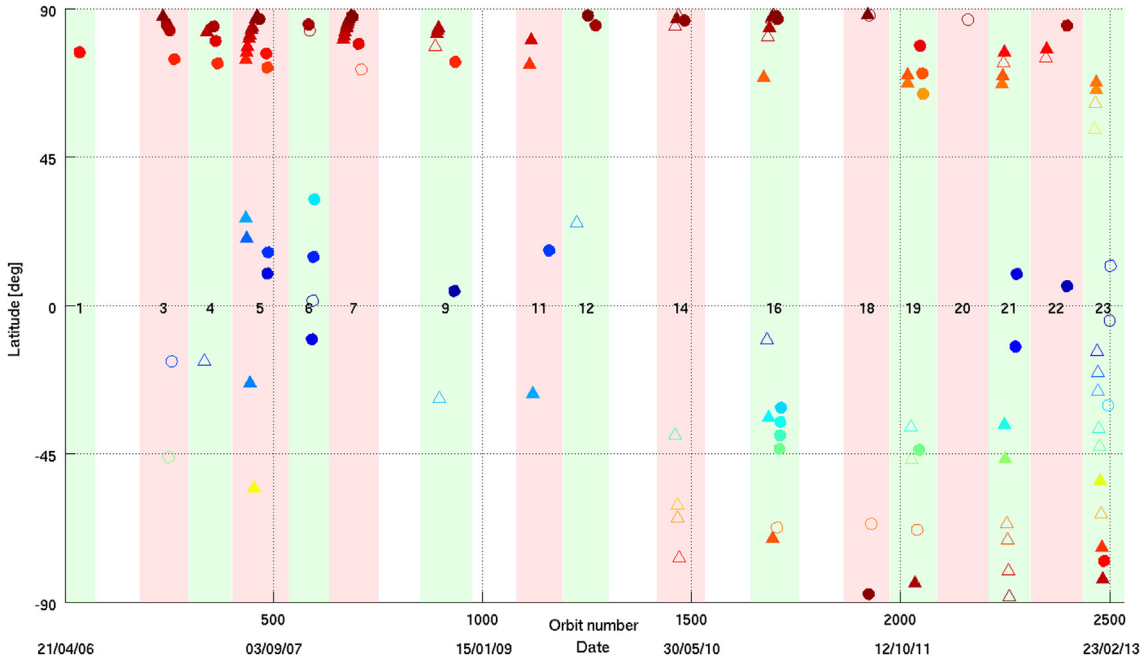

Fig. 7. Localization of the SOIR SO_2 measurements, orbit number versus latitude. The date is also given as an indication. The occultation season numbers are also given. The color code is the absolute latitude, the circles denote measurements at the morning side of the terminator, and the triangles are for the evening side. Filled markers are for positive detections of SO_2, unfilled for no detection.

Table 2
Latitude distribution of the SOIR database used in this work. Latitude symmetry relative to the Equator and terminator side symmetry are assumed here. The latitude bins are defined in order to have, in each bin, a statistically significant number of measurements as some latitudes are over- or under-represented due to the geometry of the VEX orbit. The first column is the number of positive detections, the second column is the number of measurements, and the third column gives the latitudinal density of observations, i.e. the average number of detections per latitude degree in each latitude bin.

Latitude region (°)	Number of positive detections	Number of measurements	Latitudinal density of positive detections [measurements per degree]
0–40	18	34	0.45
40–70	13	25	0.65
70–80	18	24	1.8
80–90	44	54	4.4

not plotted for clarity. They vary between 40% and 200%, with a mean value of 81%. The error bars at the bottom of the profiles tend to be larger due to the larger errors on the CO_2 density. The color code is the absolute latitude, such as in Fig. 7. The geometrical standard deviation varies between 1.5 at 0.5 mbar (~85 km) and 3 at 70 mbar (~66 km). Most of the profiles show an identical behavior: the weighted mean VMR profile calculated amongst all the profiles has a minimum at a pressure level of 1 mbar: it varies between $10^{1.92 \pm 0.83}$ ppbv – i.e. it varies of almost one order of magnitude – at 63 mbar (~65 km), $10^{1.79 \pm 0.51}$ ppbv at 1 mbar (~73 km), $10^{1.96 \pm 0.41}$ ppbv at 1 mbar (~83 km). The time variability is much larger than the mean vertical variations. The increase of the SO_2 VMR with decreasing altitude is explained by a source located at a lower altitude, resulting from the H_2SO_4 cloud droplets photo-dissociation by solar UV, see for e.g. Krasnopolsky (2012). The increase of VMR above 73 km is a controversial subject. However it has also been recently observed using SPICAV-UV solar occultations (Belyaev et al., 2012), and using ground-based observations of Venus (Moullet et al., 2013). Also, Fig. 8 of the companion paper Parkinson et al. (2015), which computes SO_2 VMR at the Venus terminator using the JPL/Caltech KINETICS 1D-photochemical model, shows a very good agreement with the SOIR VMR profiles in the 65–100 km region. A SO_2 source at higher altitude, such as an aerosol layer, could explain these VMR profiles shape, maybe coupled with a SO_2 sink in the 80–90 km region. This hypothetical source has also been suggested in Moullet et al. (2013). Furthermore, the Bougher et al. (2015) companion paper, that focuses on the comparison between the Venus Thermosphere Global Circulation Model (VTGCM) and the VAST model (Mahieux et al., 2015a), points out that such an aerosols layer may explain the temperature difference observed between the VTGCM calculations and VAST. However no agreement has been reached so far on a reasonable explanation within the Venus research community (Krasnopolsky, 2012). The SO_2 VMR variability is also very large with time and latitude, probably due to its very short photochemical lifetime (Encrenaz et al., 2012).

5.2. Latitude variations

To study the latitude variation of SO_2, mean VMR profiles are calculated for the latitude bins defined in Table 2. They are presented in Fig. 9. The colored envelopes are the weighted geometric standard deviations. It is observed that the time variations are much larger than the latitude variations.

A permanent minimum is present in the 70–76 km region, presenting weak latitude dependence, in terms of value and altitude location. It is located at a higher altitude for the equatorial bin (0–40°) than in the other bins (5 mbar, ~76 km, 45 ppbv ± 227%, $1-\sigma$ geometric standard deviation). For the mid-latitude bin (40–70°), the minimum is located at a lower altitude in the mesosphere but has the same VMR level (30 mbar, ~70 km, 47 ppbv ± 116%). The minimum of the 70–80° bin is observed at the same altitude than the mid-latitude bin, but has a slightly larger VMR value (30 mbar, ~70 km, 56 ppbv ± 128%). The minimum is less pronounced in the polar bin: it has the same VMR value as the 70–80° bin and is located at approximately the same

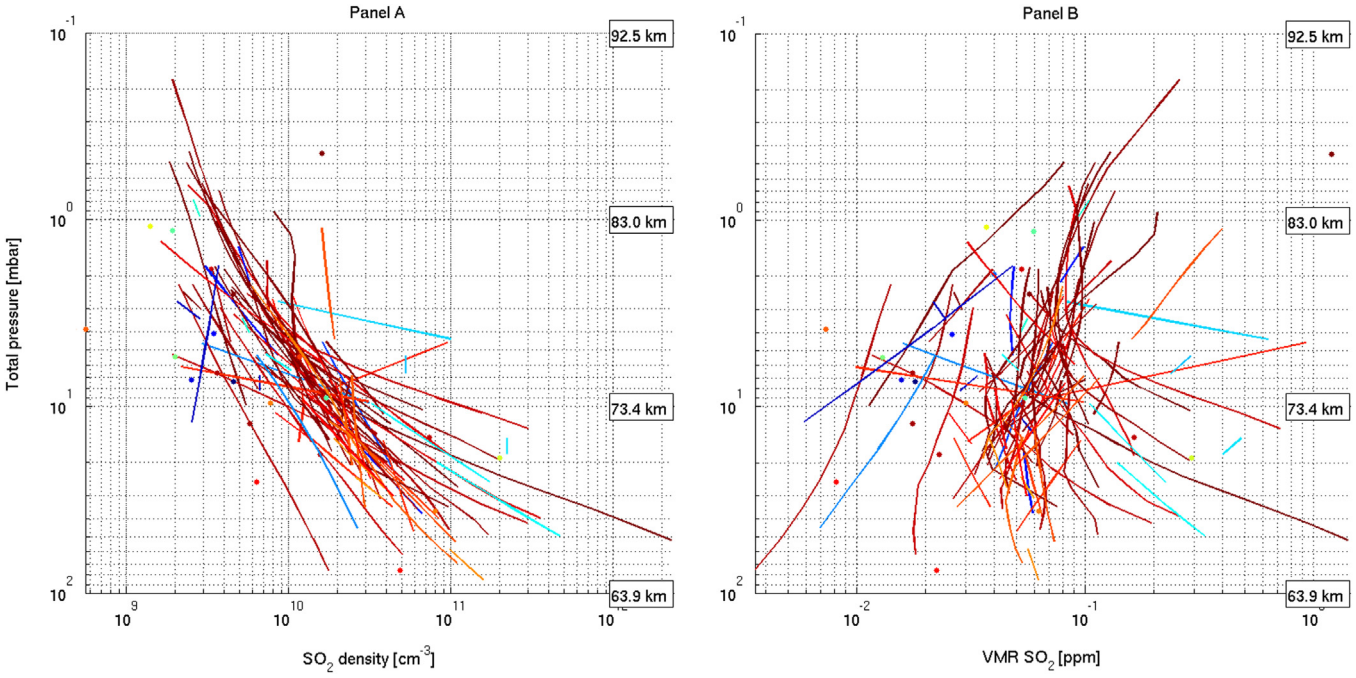

Fig. 8. SO_2 number density profiles (panel A) and SO_2 VMR profiles (panel B) as a function of the total pressure; the altitude is given on the right hand side as an indication. The points are values at single altitudes. The error bars are not plotted for clarity sake. Their values range between 40 and 200%, with a mean value of 81%. The color code is the absolute latitude.

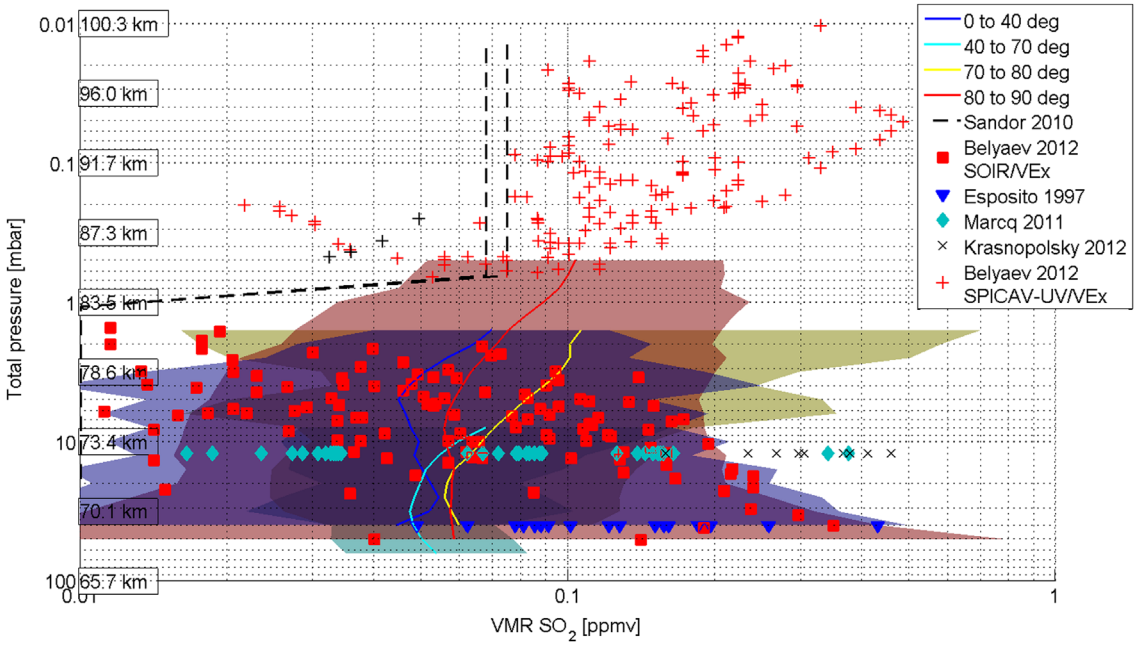

Fig. 9. SO_2 mean VMR in ppmv profiles for different latitude bins. Latitudinal symmetry about the Equator and the terminator is assumed here. The weighted standard deviations are the colored envelopes. The mean VMR profiles are calculated versus the pressure instead of the altitude to remove the mean atmosphere variations. The approximated altitudes are also given. The VMR profiles are compared to literature data (Belyaev et al., 2012; Esposito et al., 1997; Krasnopolsky, 2012; Marcq et al., 2011; Sandor et al., 2010). (For interpretation of the references to color in this figure legend, the reader is referred to the web version of this article.)

altitude as the equatorial bin (8 mbar, ~74 km, 56 ppbv ± 241%).

Above this minimum, SO_2 VMR increases with increasing altitude in all latitude bins. This trend is more pronounced in the 40–80° region than at the Poles and the equatorial region. At lower altitude, the VMR increases too. In the current dataset, almost no latitude dependence is seen below 30 mbar (~70 km). However, the few number of data at these altitudes prohibits from taking any conclusion.

Below the 10 mbar pressure level (73 km), the mean profiles from the different bins converge to nearly the same VMR value - 48–60 ppbv, with large short term variations, represented as the standard deviations. Above that pressure level, we observe a divergence of the profiles with decreasing pressure: the mid-latitude profiles have the largest SO_2 VMRs, a factor 1.5–2 larger than at other latitudes.

The mean VMR profiles have also been compared with data from the literature. There is a good agreement of the SOIR dataset

with the previously published version (Belyaev et al., 2012) obtained from the SOIR spectra (red squares): they all lie within the VMR standard deviations derived in this work. The technique described in this work allows a larger altitude coverage than the previous technique, mostly in the polar regions: the retrieval method is different, and the calibration of the instrument was improved in the meantime (Vandaele et al., 2013). Also, to calculate the VMR, the total number density profiles of Belyaev et al. (2012) were obtained using older SOIR CO_2 profiles not as accurate as the current ones. Comparisons with SPICAV-UV/VEx solar occultations (red plusses) are also presented (Belyaev et al., 2012). Even if there is almost no altitude overlaying between the two datasets, there is a good agreement between the lowest SPICAV-UV data and the highest SOIR measurements. It has to be mentionned that these SO_2 VMR profiles were obtained while fitting simultaneously SO_2 and SO. The SOIR SO_2 mean VMR profiles are also compared with Krasnopolsky (2012) mean latitude values (black crosses) obtained from ground based observations, that were derived for an altitude close to 72 km (~10 mbar). Krasnopolsky (2012) reports a latitude variation between -45° and 45°; all the values are larger and outside the SOIR standard deviations values. A comparison with Marcq et al. (2011) data (blue diamonds) obtained from nadir SPICAV-UV/VEx observations is also reported, and shows a good agreement with the SOIR data at altitude of 72 km (~10 mbar). The comparison between SOIR and Pioneer Venus Orbiter (PVO) from Esposito et al. (1997) is presented (blue triangles). They were obtained from UV observations, at an altitude of 70 km (~40 mbar). The measurements cover the whole PVO mission. They are all within the SOIR standard deviation values. The profiles are also compared with Sandor et al. (2010) results (black dashed profiles), which were obtained from ground based observations with the James Clerk Maxwell Telescope (JCMT) in the radio wavelength. This instrument is sensitive to the 70–100 km region, and covered all latitudes during that campain. Two vertical VMR profiles resulting from that campain are presented here, and the VMR values are by one order of magnitude than lower the SOIR results in the 70–83 km region. Results from (Encrenaz et al., 2012) report very large variations above the cloud top (60–80 km) across the whole disk, with values from 75 ± 25 ppbv up to 125 ± 50 ppbv, which are in perfect agreement with the SOIR measurements.

More generally, results from this study, and those from the literature studies are too complicated for a stand-alone statement about agreement, since the short term variations are very large, up to two orders of magnitude, also observed in other studies (Encrenaz et al., 2012; Marcq et al., 2011, 2013).

5.3. Long term variations

Since the SOIR database currently covers about 11 Venus years (7 Earth years), long term variations have also been investigated here. Fig. 10 presents the variations at four pressure levels. The color code is the absolute latitude, from blue (Equator) to red (Poles). The SO_2 VMR is calculated at different altitude levels corresponding to 2 mbar (~80 km), 10 mbar (~76 km), 15.8 mbar (~73 km) and 25.1 mbar (~69 km).

Most of the data points are from the polar regions, which removes the small latitudinal variations observed above the 30 mbar pressure level. The short term variations are predominant, reaching more than one order of magnitude. It is hard to conclude on any kind of long term variations of the SO_2 VMR at the 2 mbar and 10 mbar levels. At lower altitude, 15.8 mbar and 25.1 mbar pressure levels, the SO_2 seems to be slightly increasing in the polar regions from 30 ppbv around orbit 400 (26/05/2007) to 100 ppbv around orbit 1250 (22/09/2009), followed by a decrease to 40 ppbv at orbit 2500 (23/02/2013). But the amplitude of these trends is smaller than the short term variations.

The long term decay, first observed by Esposito et al. (1997) at the cloud top from PVO measurements (from 1979 till 1992), and recently reported by Marcq et al. (2013) (from 2007 till 2012) from instrument SPICAV-UV/VEx analysis, is not observed in the current dataset covering the same period of time. However, the measurements presented in this work are probably too sparse to support or contradict such a tendency, since the short term variability of SO_2 above the cloud deck is known from this study and others (Encrenaz et al., 2012; Marcq et al., 2011, 2013) to span over more than one order of magnitude.

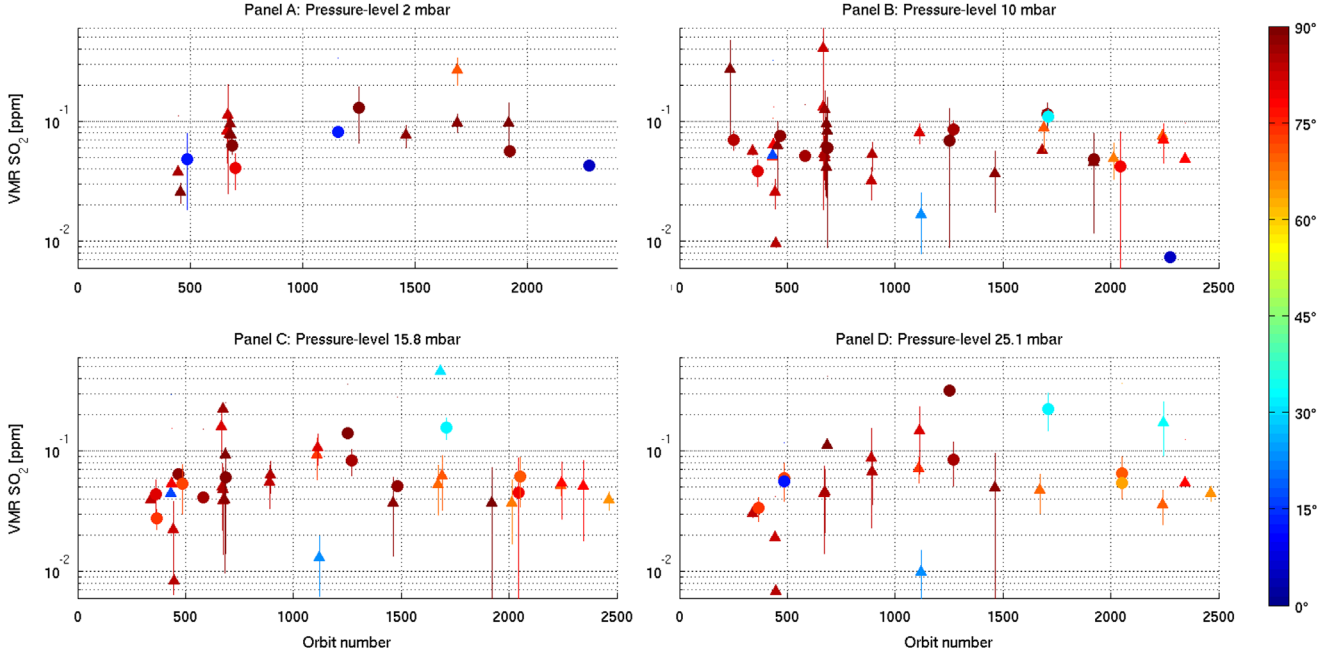

Fig. 10. Long term variations of the SO_2 VMR at four pressure levels: 2 mbar (~80 km), 5 mbar (~76 km), 10 mbar (~73 km) and 25.1 km (~69 km) in panels A–D, respectively. The color code is the latitude, see color bar on the right hand side; the uncertainties are the vertical bars. (For interpretation of the references to color in this figure, the reader is referred to the web version of this article.)

6. Conclusion

This paper reports the SO_2 measurements obtained by the SOIR instrument on board Venus Express at the Venus terminator, covering all latitudes in the 65–85 km altitude region. SO_2, one of the major and key species in the Venus photochemistry, presents a weak absorption band in the 4 μm region. No individual and isolated absorption lines are seen in the spectra measured by SOIR because of the overlapping strong CO_2 absorption. To overcome this issue and to ensure we are not just presenting upper limits, a modified version of the ASIMAT algorithm was developed. The goal of the method is to only consider positive detections when the DOF obtained by the Rodgers algorithm is meaningful. A sensitivity study has been carried out, and shows that the SNR of the spectra is an important parameter to determine a positive detection. The retrieved SO_2 profile is only weakly dependent on the a-priori profile, unless the a-priori is unrealistic compared to the actual concentration in the atmosphere.

The method has been applied to the SOIR dataset covering the May 2006–February 2013 time period. 137 occultations are considered, from which 93 positive SO_2 detections were analyzed and compiled here.

Most of the SO_2 VMR profiles show a similar shape, presenting a minimum in the 70–80 km region. A source at a lower altitude has been largely discussed in the literature, and originates from H_2SO_4 UV photo-dissociation at the clouds top. The SOIR observations would confirm the existence of a source situated at a higher altitude, previously suggested by the SPICAV-UV/VEx instrument (Belyaev et al., 2012) and also reported by Moullet et al. (2013). Attempts are currently made by atmospheric numerical photochemical modelers in order to reproduce such a vertical SO_2 distribution (Parkinson et al., 2015; Zhang et al., 2010, 2012) with fairly good results.

The latitude variation has been investigated by averaging individual VMR profiles over latitude bins. The study shows a weak altitude/latitude dependence of the VMR minima, as well as a small variation in terms of VMR values. We report an altitude of the minimum varying between 70 and 76 km; it is located at 76 km for the equatorial and polar bins, and at 70 km for the mid-latitude bins. The values range between 45 ppbv $\pm$ 227% ($1-\sigma$ standard deviation) at the Equator, 47 ppbv $\pm$ 116% in the 40–70° latitude bin, 56 ppbv $\pm$ 128% in the 70–80° latitude bin and 56 ppbv $\pm$ 241% close to the Poles.

Finally, time variations over the whole period are presented for four pressure levels, 2 mbar (~80 km), 10 mbar (~76 km), 15.8 mbar (~73 km) and 25.1 mbar (~69 km). Large variations are observed, larger than one order of magnitude, but no long-term trend is observed. At the 15.8 mbar and 25.1 mbar pressure levels, a small increase is observed between May 2007 and September 2009, with a variation between ~30 ppbv and ~100 ppbv, followed by a decrease to ~40 ppbv until February 2013. The long term variations will be further investigated through the analysis of the following observations, and in particular those at the end of 2013 during a campaign that was devoted to SO_2. Different instruments on board Venus Express and on ground have participated to this campaign, the results of which will be analyzed in near future.

Acknowledgments

Venus Express is a planetary mission from the European Space Agency (ESA). We wish to thank all ESA members who participated in the mission, in particular, H. Svedhem and D. Titov. We thank our collaborators at IASB-BIRA (Belgium), Latmos (France), and IKI (Russia). We thank CNES, CNRS, Roskosmos, and the Russian Academy of Science. The research program was supported by the Belgian Federal Science Policy Office and the European Space Agency (ESA, PRODEX program, Contracts C 90268, 90113, and 17645). We acknowledge the support of the "Interuniversity Attraction Poles" program financed by the Belgian government (Planet TOPERS). The research leading to these results has received funding from the European Union Seventh Framework Program (FP7/2007–2013) under Grant agreement no. 606798. A. Mahieux thanks the FNRS for the position of "chargé de recherche". D. Belyaev acknowledges the grant 11.G34.31.0074 from the Russian government and the program 22 from the RAS. The authors acknowledge the support provided by ISSI, through the organization of the International Team "Sulfur Dioxide Variability in the Venus Atmosphere" (http://www.issibern.ch/teams/venusso2/).

References

Barker, E.S., 1979. Detection of SO_2 in the UV spectrum of Venus. Geophys. Res. Lett. 6, 117–120.

Belyaev, D., Korablev, O., Fedorova, A., Bertaux, J.L., Vandaele, A.C., Montmessin, F., Mahieux, A., Wilquet, V., Drummond, R., 2008. First observations of SO_2 above Venus' clouds by means of solar occultation in the infrared. J. Geophys. Res., 113. http://dx.doi.org/10.1029/2008JE003143.

Belyaev, D., Montmessin, F., Bertaux, J.L., Mahieux, A., Fedorova, A., Korablev, O., Marcq, E., Yung, Y., Zhang, X., 2012. Vertical profiling of SO_2 and SO above Venus' clouds by SPICAV/SOIR solar occultations. Icarus 217, 740–751.

Bertaux, J.L., Vandaele, A.C., Korablev, O., Villard, E., Fedorova, A., Fussen, D., Quémerais, E., Belyaev, D., Mahieux, A., Montmessin, F., Müller, C., Neefs, E., Nevejans, D., Wilquet, V., Dubois, J.P., Hauchecorne, A., Stepanov, A., Vinogradov, I., Rodin, A., Team, A.T.S, 2007. A warm layer in Venus' cryosphere and high altitude measurements of HF, HCl, H_2O and HDO. Nature 450, 646–649 http://dx.doi.org/610.1038/nature05974.

Bézard, B., Baluteau, J.P., Marten, A., Coron, N., 1987. The $^{12}C/^{13}C$ and $^{16}O/^{18}O$ ratios in the atmosphere of Venus from high-resolution 10-mum spectroscopy. Icarus 72, 623–634.

Bougher, S.W., Brecht, A., Schulte, R., Fischer, J., Parkinson, C., Mahieux, A., Wilquet, V., Vandaele, A.C., 2015. Upper atmosphere temperature structure at the venusian terminators: a comparison of SOIR and VTGCM results. Planet. Sp. Sci. 113–114, 337–347.

Clancy, R.T., Muhleman, D.O., 1991. Long-term (1979–1990) changes in the thermal, dynamical and compositional structure of the Venus mesosphere as inferre from microwave spectral line observations of ^{12}CO, ^{13}CO, and $C^{18}O$. Icarus 89, 129–146.

Encrenaz, T., Greathouse, T., Roe, H., Richter, M., Lacy, J., Bézard, B., Fouchet, T., Widemann, T., 2012. HDO and SO_2 thermal mapping on Venus: evidence for strong SO_2 variability. Astron. Astrophys. 543, http://dx.doi.org/10.1051/0004-6361/201219419 (Article no. A153).

Esposito, L.W., Bertaux, J.L., Krasnopolsky, V., Moroz, V.I., Zasova, L.V., 1997. Venus II: Geology, Geophysics, Atmosphere, and Solar Wind Environment. In: Bougher, S.W., Hunten, D.M., Phillips, R.J. (Eds.), Chemistry of lower atmosphere and clouds. University of Arizona Press, Tucson, AZ, pp. 415–458.

Esposito, L.W., Copley, M., Eckert, R., Gates, L., Stewart, A.I.F., Worden, H., 1988. Sulfur dioxide at the Venus cloud tops, 1978–1986. J. Geophys. Res. 93, 5267–5276.

Fedorova, A., Korablev, O., Vandaele, A.C., Bertaux, J.L., Belyaev, D., Mahieux, A., Neefs, E., Wilquet, V., Drummond, R., Montmessin, F., Villard, E., 2008. HDO and H_2O vertical distributions and isotopic ratio in the Venus mesosphere by Solar Occultation at Infrared spectrometer onboard Venus Express. J. Geophys. Res. 113, http://dx.doi.org/10.1029/2008JE003146 (Article no. E00B22).

Fegley Jr., B., Klingelhöfer, G., Lodders, K., Widemann, T., 1997. Geochemistry of surface-atmosphere interactions on Venus. In: Bougher, S.W., Hunten, D.M., Phillips, R.J. (Eds.), Venus II. The University of Arizona Press, Tucson, pp. 591–636.

Hedin, A.E., Niemann, H.B., Kasprzak, W.T., 1983. Global empirical model of the Venus thermosphere. J. Geophys. Res. 88, 73–83.

Jessup, K.L., Mills, F., Marcq, E., Bertaux, J.L., Roman, T., Yung, Y., 2012. Coordinated HST, Venus Express, and Venus Climate Orbiter Observations of Venus, VEXAG, NASA program 12433, Washington, DC.

Krasnopolsky, V.A., 2012. A photochemical model for the Venus atmosphere at 47–112 km. Icarus 218, 230–246.

Mahieux, A., Berkenbosch, S., Clairquin, R., Fussen, D., Mateshvili, N., Neefs, E., Nevejans, D., Ristic, B., Vandaele, A.C., Wilquet, V., Belyaev, D., Fedorova, A., Korablev, O., Villard, E., Montmessin, F., Bertaux, J.L., 2008. In-flight performance and calibration of SPICAV/SOIR on-board Venus Express. Appl. Opt. 47, 2252–2265.

Mahieux, A., Vandaele, A.C., Bougher, S.W., Drummond, R., Robert, S., Chamberlain, S., Wilquet, V., Piccialli, A., Montmessin, F., Tellmann, S., Pätzold, M., Häusler, B., Bertaux, J.L., 2015a. Update of the Venus density and temperature profiles at high altitude measured by SOIR on board Venus Express. Planet. Sp. Sci. 113–114, 310–321.

Mahieux, A., Vandaele, A.C., Drummond, R., Robert, S., Wilquet, V., Fedorova, A., Bertaux, J.L., 2010. Densities and temperatures in the Venus mesosphere and lower thermosphere retrieved from SOIR onboard Venus Express: retrieval technique. J. Geophys. Res. 115, http://dx.doi.org/10.1029/2010JE003589 (Article no. E12014).

Mahieux, A., Vandaele, A.C., Robert, S., Wilquet, V., Drummond, R., Bertaux, J.L., 2015b. Halogens measurements in the Venus upper atmosphere retrieved from SOIR on board Venus Express. Planet. Sp. Sci. 113–114, 265–275.

Mahieux, A., Vandaele, A.C., Robert, S., Wilquet, V., Drummond, R., Montmessin, F., Bertaux, J.L., 2012. Densities and temperatures in the Venus mesosphere and lower thermosphere retrieved from SOIR on board Venus Express: carbon dioxide measurements at the Venus terminator. J. Geophys. Res. 117, http://dx.doi.org/10.1029/2012JE004058 (Article no. E07001).

Mahieux, A., Wilquet, V., Drummond, R., Belyaev, D., Fedorova, A., Vandaele, A.C., 2009. A new method for determining the transfer function of an acousto optical tunable filter. Opt. Express 17, 2005–2014.

Marcq, E., Belyaev, D., Montmessin, F., Fedorova, A., Bertaux, J.L., Vandaele, A.C., Neefs, E., 2011. An investigation of the SO_2 content of the venusian mesosphere using SPICAV-UV in nadir mode. Icarus 211, 58–69.

Marcq, E., Bertaux, J.L., Montmessin, F., Belyaev, D., 2013. Variations of sulphur dioxide at the cloud top of Venus's dynamic atmosphere. Nat. Geosci. 6, 25–28.

Marcq, E., Bézard, B., Drossart, P., Piccioni, G., Reess, J.M., Henry, F., 2008. A latitudinal survey of CO, OCS, H_2O, and SO_2 in the lower atmosphere of Venus: spectroscopic studies using VIRTIS-H. J. Geophys. Res. 113, http://dx.doi.org/10.1029/2008JE003074 (Article no. E00B07).

Moullet, A., Moreno, R., Encrenaz, T., Lellouch, E., Fouchet, T., 2013. Submillimeter spectroscopy of Venus's atmosphere with ALMA: CO, HDO, and sulfur species. DPS (Division for Planetary Sciences) 45th Annual Meeting, Boulder, Colorado.

Nevejans, D., Neefs, E., Van Ransbeeck, E., Berkenbosch, S., Clairquin, R., De Vos, L., Moelans, W., Glorieux, S., Baeke, A., Korablev, O., Vinogradov, I., Kalinnikov, Y., Bach, B., Dubois, J.P., Villard, E., 2006. Compact high-resolution space-borne echelle grating spectrometer with AOTF based on order sorting for the infrared domain from 2.2 to 4.3 μm. Appl. Opt. 45, 5191–5206.

Parkinson, C., Yung, Y., Esposito, L., Gao, P., Bougher, S.W., Hirtzig, M., 2014. Photochemical control of the distribution of venusian water and comparison to Venus Express SOIR observations. Planet. Sp. Sci.

Rodgers, C.D., 2000. Inverse Methods for Atmospheric Sounding: Theory and practice, University of Oxford, Singapore.

Rothman, L.S., 1981. AFGL atmospheric absorption line parameters compilation: 1980 version. Appl. Opt. 20, 791–795.

Rothman, L.S., Gordon, I.E., Babikov, Y., Barbe, A., Benner, D.C., Bernath, P.F., Bizzocchi, L., Boudon, V., Brown, L.R., Campargue, A., Chance, K.V., Cohen, E. A., Coudert, L.H., Devi, V.M., Drouin, B.J., Fayt, A., Flaud, J.-M., Gamache, R., Harrison, J.J., Hartmann, J.M., Hill, C., Hodges, J., Jacquemart, D., Jolly, A., Lamouroux, J., LeRoy, R.J., Li, G., Long, D.A., Lyulin, O.M., Mackie, C.J., Massie, S., Mikhailenko, S., Muller, H.S.P., Naumenko, O., Nikitin, A., Orphal, J., Perevalov, V., Perrin, A., Polovtseva, E.R., Richard, C., Smith, M.A.H., Starikova, E., Sung, K., Tashkun, S., Tennyson, J., Toon, G., Tyuterev, V.G., Wagner, G., 2013. The HITRAN2012 molecular spectroscopic database. J. Quant. Spectrosc. Radiat. Transf. 130, 4.

Rothman, L.S., Jaquemart, D., Barbe, A., Benner, C., Birk, M., Brown, L.R., Carleer, M., Chackerian Jr., C., Chance, K.V., Coudert, L.H., Dana, V., Devi, M., Flaud, J.-M., Gamache, R.B., Goldman, A., Hartmann, J.-M., Jucks, K.W., Maki, A.G., Mandin, J.-Y., Massie, S.T., Orphal, J., Perrin, A., Rinsland, C.P., Smith, M.A.H., Tennyson, J., Tolchenov, R.N., Toth, R.A., Vander Auwera, J., Varanasi, P., Wagner, G., 2005. The HITRAN 2004 molecular spectroscopic database. J. Quant. Spectrosc. Radiat. Transf. 96, 139–204.

Sandor, B., Clancy, R.T., Moriarty-Schieven, G., 2007. SO and SO_2 in the Venus Mesosphere: observations of extreme and rapid variation. Bull. Am. Astron. Soc. 39, 503.

Sandor, B., Clancy, R.T., Moriarty-Schieven, G., 2012. Upper limits for H_2SO_4 in the mesosphere of Venus. Icarus 217, 839–844.

Sandor, B.J., Clancy, R.T., Moriarty-Schieven, G., Mills, F.P., 2010. Sulfur chemistry in the Venus mesosphere from SO_2 and SO microwave spectra. Icarus 208, 49–60.

Vandaele, A.C., Mahieux, A., Robert, S., Berkenbosch, S., Clairquin, R., Drummond, R., Letocart, V., Neefs, E., Ristic, B., Wilquet, V., Colomer, F., Belyaev, D., Bertaux, J.L., 2013. Improved calibration of SOIR/Venus Express spectra. Opt. Express 21, 21148.

Vandaele, A.C., Mahieux, A., Robert, S., Drummond, R., Wilquet, V., Bertaux, J.L., 2015. Carbon monoxide short term variability observed on Venus with SOIR/VEX. Planet. Sp. Sci. 113–114, 238–256. http://dx.doi.org/10.1016/j.pss.2014.12.012.

Zasova, L.V., Moroz, V.I., Linkin, V.M., Khatountsev, I.A., Maiorov, B.S., 2006. Structure of the venusian atmosphere from surface up to 100 km. Cosm. Res. 44, 364–383.

Zhang, X., Liang, M., Mills, F., Belyaev, D., Yung, Y., 2012. Sulfur chemistry in the middle atmosphere of Venus. Icarus 217, 714–739.

Zhang, X., Liang, M.C., Montmessin, F., Bertaux, J.L., Parkinson, C., Yung, Y.L., 2010. Photolysis of sulphuric acid as the source of sulphur oxides in the mesosphere of Venus. Nat. Geosci. 3, 834–837.